Selective Amplification of the Primary Exciton in a MoS_2 Monolayer

Hyun Seok Lee,[1,*] Min Su Kim,[1] Youngjo Jin,[1,2] Gang Hee Han,[1] Young Hee Lee,[1,2,3,†] and Jeongyong Kim[1,2,‡]
[1]Center for Integrated Nanostructure Physics (CINAP), Institute for Basic Science (IBS), Sungkyunkwan University, Suwon 440-746, Korea
[2]Department of Energy Science, Sungkyunkwan University, Suwon 440-746, Korea
[3]Department of Physics, Sungkyunkwan University, Suwon 440-746, Korea
(Received 4 March 2015; published 25 November 2015)

Optoelectronics applications for transition-metal dichalcogenides are still limited by weak light absorption and their complex exciton modes are easily perturbed by varying excitation conditions because they are inherent in atomically thin layers. Here, we propose a method of selectively amplifying the primary exciton (A^0) among the exciton complexes in monolayer MoS_2 via cyclic reexcitation of cavity-free exciton-coupled plasmon propagation. This was implemented by partially overlapping a Ag nanowire on a MoS_2 monolayer separated by a thin SiO_2 spacer. Exciton-coupled plasmons in the nanowire enhance the A^0 radiation in MoS_2. The cumulative amplification of emission enhancement by cyclic plasmon traveling reaches approximately twentyfold selectively for the A^0, while excluding other B exciton and multiexciton by significantly reduced band filling, without oscillatory spectra implying plasmonic cavity effects.

DOI: 10.1103/PhysRevLett.115.226801 PACS numbers: 73.20.Mf, 71.35.-y, 78.55.Ap, 73.21.-b

Two advantages of two-dimensional transition-metal dichalcogenide (TMD) semiconductors in two-dimensional optoelectronics are band-gap tuning via controlling atomic layers and hybridizations, and on-chip integration via direct growth [1–4]. Manipulating exciton emissions by controlling light-emitter interactions is key to exciton engineering [5]. However, their inherent drawback is weak light absorption by their atomically thin layer [6]. The use of the local-field enhancement effect of localized surface plasmons via hybridization with metal nanostructures is a promising way to enhance the optoelectronic performance of TMDs [1,6–8]. However, this approach is challenging because coherent tuning between the plasmon resonance and the optical wavelength must be precisely engineered [7–10], and the mechanism of the interaction between surface plasmon polaritons (SPPs) and the intricate excitons of TMDs must be understood [11–17].

Here, we propose a cavity-free method to enhance the exciton emission performance of TMD semiconductors under varying excitation laser power (P_{ex}) without sacrificing peak quality and shape. We used nanowire (NW)-TMD emitter hybrids in this study (Methods [18]). The Ag-NW partly overlapping on the monolayer MoS_2 from which it was separated by a SiO_2 (10 nm) spacer to prevent band-pinning, doping, and photoluminescence (PL) quenching from direct metal-semiconductor contact [30,31]. Figure 1(a) shows a schematic and cross-sectional view of the experimental setup. A^0 (primary A exciton, ~1.88 eV), A' (multiexciton, ~1.84 eV), and B (B exciton, ~2.02 eV) indicate typical exciton complexes of MoS_2 monolayers [11,13–15]. "On NW" is the NW-MoS_2 overlapping region (NMOR), and "off NW" is the bare MoS_2 region.

The PL image in Fig. 1(b) exhibits strong red emission at the laser input position (LIP) indicated by a green arrow and weak but still prominent emission at the NW-end position (NWEP), implying that MoS_2 excitons are coupled to SPPs and propagate along the NW [31–33]. The PL signals were collected at the same LIP indicated by a white arrow. Figure 1(c) shows the normalized PL spectra that were deconvoluted using a Lorentzian function. The unknown X peak for off NW is presumably a localized state due to defects or impurities [34]. At all five P_{ex} levels (5–500 μW), only the A^0 observation for on NW is markedly different from the PL spectra for off NW which have three exciton modes. For on NW, the A-peak position of ~1.88 eV and full width at half maximum of ~50 meV remain unchanged and independent of P_{ex}. However, for off NW, as P_{ex} increases, the A-peak center position redshifts considerably because the A' dominates the A peak, and the intensities of A' and B increase.

Figure 1(d) compares the PL spectra for on NW and off NW at $P_{ex} = 100$ μW. Notably, the A-peak intensity (I_A) for on NW consisting of only the A^0 is dramatically enhanced compared with that for off NW consisting of the A^0 and A' [Fig. 1(c)]. The A-peak enhancement factor is defined as $\varepsilon = I_{PL}^{on}/I_{PL}^{off}$, where I_{PL}^{on} and I_{PL}^{off} are the maximum I_A for on NW and off NW, respectively, and the ε factor can reach ~20. Figure 1(e) shows the log-log scale intensity-power curves for A and B peaks in off NW. The integrated PL intensity (I_{PL}) is approximately equal to $(P_{ex})^m$, where m denotes exponent. For the I_A, $m \sim 0.9$ at $P_{ex} = 5$–100 nW, where only the A^0 is identified via a single Lorentzian fit (SLF) [Fig. 1(f)]. However, at $P_{ex} > 100$ nW, the I_A is saturated and m is degraded to ~0.6 as the A' starts to evolve and dominate the A peak

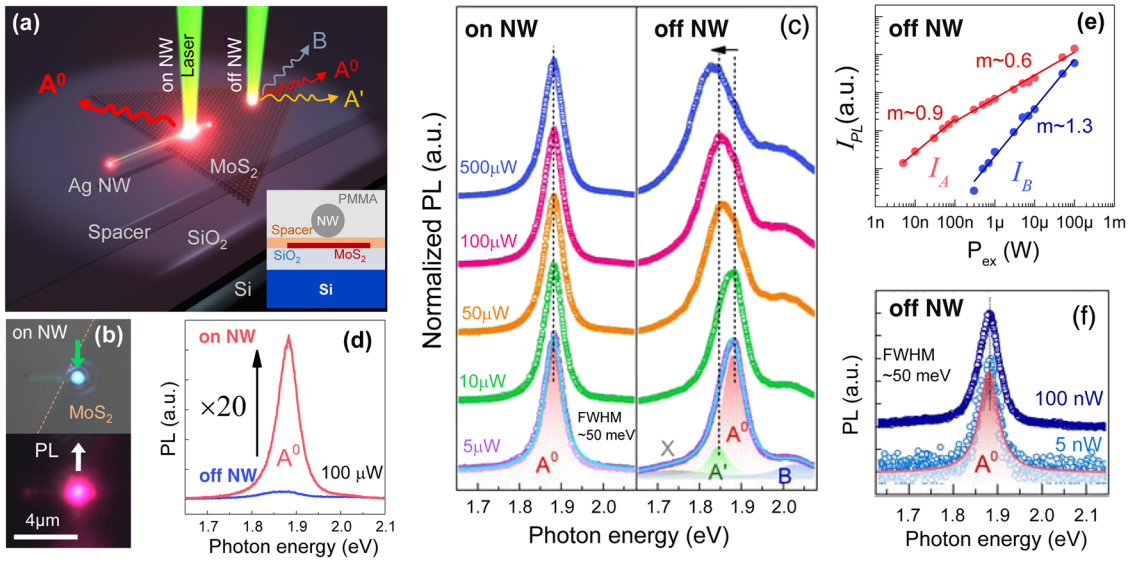

FIG. 1 (color online). (a) Schematic of the experimental setup with a side view of the hybrid. PL signals were collected from the NMOR (on NW) and from the bare MoS_2 (off NW) that were excited by an input laser. (b) (top) Optical micrograph showing the LIP (green arrow) and (bottom) PL image showing the collection position (white arrow) of the PL signal at the same LIP. NW length, ~4 μm. Effective NW length from the NWEP to the LIP, ~3 μm. (c) Normalized PL signals as a function of P_{ex} for on NW and off NW, with examples of Lorentzian deconvolution at $P_{ex} = 5$ μW. (d) PL spectra for on NW and off NW at $P_{ex} = 100$ μW. (e) The log-log scale PL intensity (I_{PL}) as a function of P_{ex} derived from the PL spectra for off NW. (f) The PL spectra for off NW at $P_{ex} = 5$ nW and 100 nW and SLF for $P_{ex} = 5$ nW identified as A^0.

[Fig. 1(c), off NW]. As the A peak starts being saturated over 100 nW, the B-peak intensity (I_B) also starts to emerge and increase in response to P_{ex} with $m \sim 1.3$. Therefore, for off NW, the exclusive emergence of the A^0 at extremely low P_{ex} [Fig. 1(f)] strongly contrasts with the formation of exciton complexes (A' and B) at high P_{ex} [Fig. 1(c)]; this is attributed to the result of the band-filling effect for excitons [35–38]. Details are given in Note 1 [18]. Moreover, because the full width at half maximum (~50 meV) for off NW at low P_{ex} [Fig. 1(f)] is the same as that for on NW [Fig. 1(c)], the origin of PL enhancement (PLE) for on NW [Fig. 1(d)] cannot be associated with the cavity resonance effect revealing oscillatory fringes [39].

To determine the role of NWs in A^0 enhancement, the NW length effect was investigated in fully and partially overlapping NW samples, where the PL signals were collected at the same LIP. x_M is the length of the fully overlapping NW (FONW), while for the partially overlapping NW (PONW), x is the effective length of bare NW measured from the NWEP to the LIP [Fig. 2(a)]. The ε factors were measured for numerous devices [Fig. 2(b)]. For FONW samples, the ε factors (mean ~1.3) were appreciably negligible for various x_M values (Sec. 1 [18]). However, for the PONW samples, the considerable enhancement (~20 times for $x \sim 3$ μm) decayed exponentially (decay length ~6 μm) as a function of x despite the significant fluctuation in ε values, which is attributed to the variable sample conditions, i.e., NW quality, laser focusing, and SPP reflectivity at the NWEP (Sec. 4 [18]). The lack of x_M dependence of the ε factor in the FONW samples implies that the selective A^0 enhancement is associated with longitudinal-mode SPP (L-SPP) propagation along the x.

To characterize the propagation behavior of exciton-coupled (EC)-SPPs in NWs, PL signals for longer NWs ($x \sim 6.5$ μm) were collected at the LIP [Fig. 3(b)] and at NWEP [Fig. 3(c)] during laser illumination at the NMOR. In Fig 3(a), the left image indicates the LIP (green arrow) and the right image indicates the PL collecting positions for the LIP and the NWEP (white arrows). At the LIP, the ε

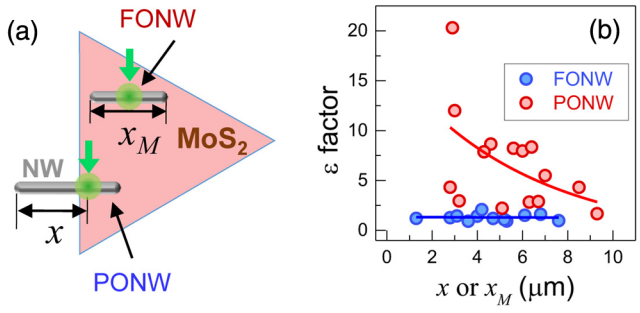

FIG. 2 (color online). (a) Schematics for two different sample configurations: fully overlapping NW (FONW) and partially overlapping NW (PONW) on MoS_2 flakes. x_M, the length of the FONW. x, the effective length for the PONW from the end of the bare NW to the LIP (green arrow). (b) ε factor (maximum I_A for on NW divided by that of off NW) as a function of x or x_M. At $P_{ex} = 100$ μW, the PL signals were collected at the same LIP for numerous devices with the two different sample configurations.

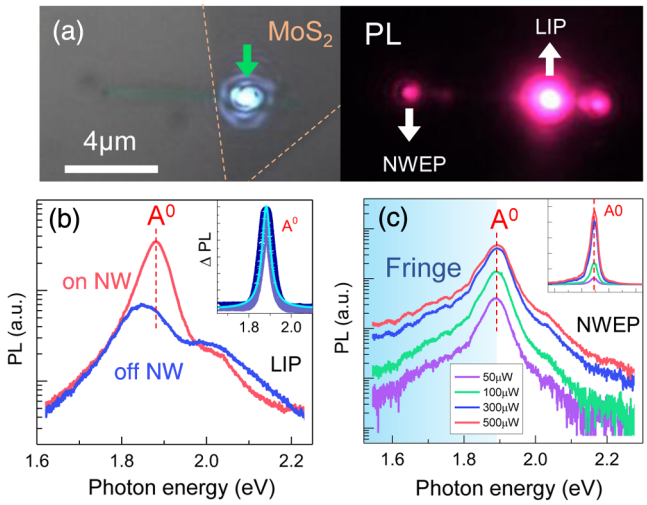

FIG. 3 (color online). (a) Optical micrograph (left) illustrating MoS_2 flake position and PL image (right). x, ~6.5 μm; NW length, ~8 μm; green arrow, LIP; white arrow, PL signal collection position. (b) PL spectra collected at the LIP. Log-scale PL spectra comparison between on NW and off NW with an ε factor of ~7 at $P_{ex} = 500$ μW. Inset, PL for off NW subtracted from that of on NW and its SLF identified as A^0 implying only A^0 enhancement for on NW. (c) PL spectra collected at the NWEP as a function of P_{ex}. Log-scale PL spectra reveal oscillatory fringes that are apparent at $\hbar\omega < \hbar\omega_{A0}$. Inset, linear scale.

factor reaches ~7 selectively for the A^0 [Fig. 3(b)]. The A^0 selectivity is confirmed by subtracting the PL spectrum for off NW from that of on NW (which yields ΔPL) and the A^0 is identified exclusively via a SLF [Fig. 3(b), inset].

In linear-scale PL spectra collected at the NWEP [Fig. 3(c), inset], the A^0 also dominates the A peak for all P_{ex}. Interestingly, the log-scale plot of the spectra [Fig. 3(c)] shows oscillatory fringes at photon energy lower than that of A^0 ($\hbar\omega < \hbar\omega_{A0}$) and no fringes at $\hbar\omega \geq \hbar\omega_{A0}$. The SPPs with $\hbar\omega < \hbar\omega_{A0}$ (involving A') coupled from the A-peak tail form Fabry-Pérot cavity modes of poor quality (Sec. 2 [18]) in which excitons travel through NWs as standing waves that generally accompany oscillatory spectra [9,31]. This cavity signal is observed only at the NWEP, because the scattering of L-SPPs is negligible at the LIP (midsection of NW) with the symmetrical NW geometry in the axial direction (Sec. 3 [18]). Conversely, at the NMOR, the SPPs with $\hbar\omega \geq \hbar\omega_{A0}$ are reabsorbed into the MoS_2 layer after their round-trip and then lose their energies by PL emission in MoS_2 (Secs. 4 and 5 [18]); thus, the cavity modes are not constructed. Although the SPPs with $\hbar\omega < \hbar\omega_{A0}$ exhibit some cavity effect, they do not contribute to A^0 amplification because they are not absorbed by the MoS_2 layer. Therefore, this selective A^0 amplification phenomenon at the LIP differs from the PLE via the plasmonic antenna effect [1,8] (Sec. 4 [18]) or the conventional cavity effect [9,31].

Remarkably, the PONWs play a key role in selective A^0 enhancement. Furthermore, this enhancement becomes more prominent as x decreases. In Fig. 4(a), the input laser generates excitons in the MoS_2 and the excitons couple with SPPs in the NW. The EC-SPPs propagate through the NW and return to their LIP after plasmon Ohmic loss in the NW, which is the result of the imaginary part of the dielectric function of Ag and loss due to scattering at the NWEP [40]. The SPPs returned to their LIP enhance the spontaneous emission (SE) rate of the generated MoS_2 excitons, resulting in a gain in exciton emission ($\gamma > 1$) [41]. The SE enhancement via plasmonic resonant coupling with a metal nanostructure is known as the Purcell enhancement (PE) effect [10]. Conversely, SPPs with a tightly confined mode enhance SE due to the nonresonant PE effect, even without the longitudinal cavity effect [10,41]. The nonresonant PE factor is given by

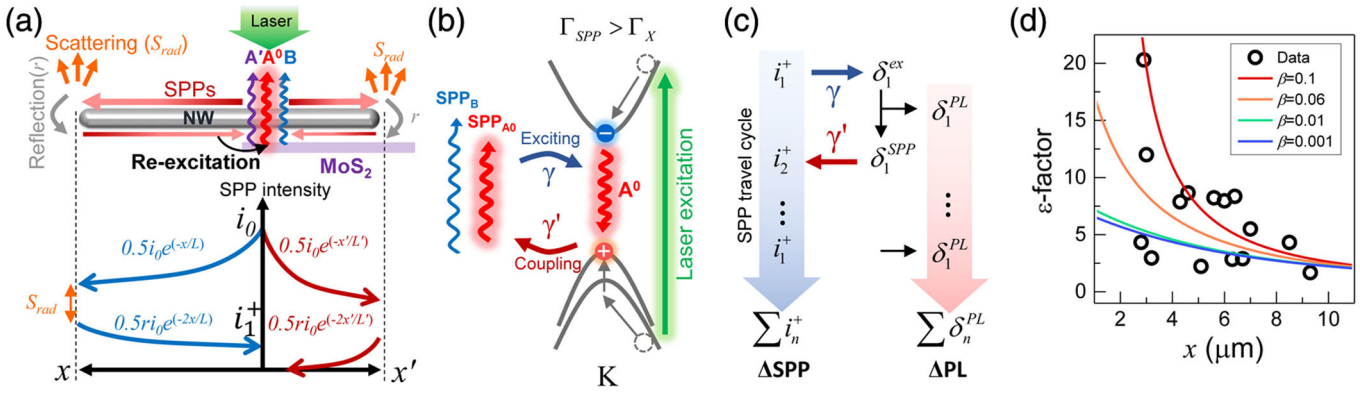

FIG. 4 (color online). (a) Complex excitons (A^0, A', and B) excited under an intense laser coupled to the SPPs at the LIP. The traveling SPPs lose their intensity via Ohmic loss along the NW and scattering loss (S_{rad}) at the NWEP. Reflected SPPs selectively reexcite only the A^0. (b) SPP cyclic traveling enhances the A^0 emission by restricting the band-filling effect in MoS_2 excitons. (c) PL and SPP amplification flow via repeated interaction between excitons and SPPs as the traveling cycles increase. (d) Comparison of the experimental data for the PONW samples in Fig. 2(b) with the plots of Eq. (1) for various β as a function of x.

$F_{NP} = \Gamma_{SPP}/\Gamma_X \propto (\lambda_e/d)^3$, where Γ_{SPP} and Γ_X are the radiative decay rate for on NW and off NW, respectively; λ_e is the exciton wavelength in free space, and d is the thickness of spacer [32,41]; and thus, $\gamma \propto F_{NP}$. Because $\Gamma_{SPP} > \Gamma_X$, the enhanced SE can restrict the band-filling effect (Notes 1 and 2 [18]). Therefore, mostly the A^0 is generated for on NW, as discussed in Fig. 1.

The enhanced A^0 emission due to the returned SPPs recouples to the SPPs at NMOR, resulting in SPP intensity enhancement (SPP enhancement factor, $\gamma' > 1$) [9,42]. This agrees with the A^0 dominance in the EC-SPPs monitored at the NWEP [Fig. 3(c)]. Therefore, the accumulation of selective A^0 reexcitation via cyclic round-trips of the SPPs significantly amplifies the A^0 intensity at their LIP through the repeated PL gain process [Figs. 4(b) and 4(c)]. Details of the analytical model are given in Note 2 [18]. The EC-SPPs from the MoS_2 layer via laser excitation, defined as i_0, propagate along the left (x) and the right (x', NMOR) regions of the NW and undergo SPP Ohmic loss, which is proportional to $0.5i_0e^{(-x/L)}$ and $0.5i_0e^{(-x'/L')}$, respectively, where L and L' are the decay lengths of the SPPs in the x and x' directions, respectively, and the factor of 0.5 is applied because it is assumed that the equivalent amount of SPPs travel in each NW direction [Fig. 4(a)]. In this situation, the SPPs that are coupled directly with the input laser at the NW midsection are ignored, because L-SPPs are not activated as they are at the NWEP [43] (Secs. 3 and 4 [18]). The EC-SPPs are reflected at the NWEP with a reflectivity of $r \sim 0.25$ and returned to the LIP [40].

The intensity of the returned SPPs after one round-trip is given by $i_1^+ = 0.5ri_0e^{(-2x/L)} + 0.5ri_0e^{(-2x'/L')}$. We assumed $L \gg L'$ due to the additional loss of SPPs resulting from their reabsorption and reemission in the MoS_2 layer during propagation along the x' direction (Sec. 5 [18]). Therefore, $i_1^+ \sim 0.5ri_0e^{(-2x/L)} = i_0g$. Figure 4(c) shows the amplification flow via repeated interaction between excitons and SPPs as the number of SPP traveling cycles increases. The i_1^+ reexcites additional exciton (δ_1^{ex}) in MoS_2 and $\delta_1^{ex} = \gamma i_1^+$. $\delta_1^{ex} = \delta_1^{PL} + \delta_1^{SPP}$, where $\delta_1^{PL} = (1-\rho)\delta_1^{ex}$ is the enhanced PL and $\delta_1^{SPP} = \rho\delta_1^{ex} = \rho\gamma'(\gamma i_1^+)$ is recoupled to SPPs with enhanced intensity (γ') for the second round of travel, where $\rho < 1$ denotes the partial ratio of δ_1^{ex}. After n travel cycles, the total SPP intensity enhancement and the total PLE are given by $\Delta i^+ = i_0g\sum_{n=0}^{\infty}(\gamma'\gamma\rho g)^n$ and $\Delta\delta^{PL} = (1-\rho)\gamma i_0g\sum_{n=0}^{\infty}(\gamma'\gamma\rho g)^n$, respectively. From the simulation result, $L \sim 12$ μm for the A^0 (Sec. 3 [18]). When $x > 3$ μm, $g < \sim 0.08 \ll 1$. For convergence, $\gamma'\gamma\rho g < 1$. By Taylor expansion, $\sum_{n=0}^{\infty}(\gamma'\gamma\rho g)^n \sim 1/(1-\gamma'\gamma\rho g)$, so $\Delta\delta^{PL} \sim (1-\rho)\gamma i_0g/(1-\gamma'\gamma\rho g)$ and $\Delta i^+ \sim i_0g/(1-\gamma'\gamma\rho g)$. For the first SPP propagation, the SPP intensity is given by $i_1^s = (1-r)0.5i_0e^{(-x/L)} = i_0g'$. After n travel cycles, the total scattered SPPs at the NWEP is given by $\Delta i^s = i_0g'\sum_{n=0}^{\infty}(\gamma'\gamma\rho g)^n \sim i_0g'/(1-\gamma'\gamma\rho g)$. Because the ΔPL intensity at the LIP is stronger than that of the scattered SPPs at the NWEP by more than twentyfold [Fig. 3], $\Delta\delta^{PL}/\Delta i^s \sim (1-\rho)\gamma i_0g/(i_0g') \sim 20$, which yields $\gamma \sim C/(1-\rho)$ with $C \sim 100$. Eventually, $\Delta\delta^{PL} \sim Ci_0g/(1-C\beta g)$, where $\beta = \gamma'\rho/(1-\rho)$. The exciton-SPP conversion efficiency was determined experimentally as $\eta = i_0/(I_{PL}^{off} + i_0) \sim 0.32$ [33], and thus $i_0 = \eta/(1-\eta)I_{PL}^{off} \sim 0.5I_{PL}^{off}$. The ε factor is approximated as

$$\varepsilon = \frac{I_{on}^{PL}}{I_{off}^{PL}} \sim \frac{I_{off}^{PL} + \Delta\delta^{rad}}{I_{off}^{PL}} \sim 1 + \frac{Ci_0g}{1 - C\beta g I_{off}^{PL}} \sim 1 + \frac{6.4e^{-x/6}}{1 - 12.9\beta e^{-x/6}}. \quad (1)$$

Figure 4(d) presents the experimental data for the PONW samples from Fig. 2(b) and plots of Eq. (1) in response to various β. With β in the range of $0.001 \le \beta \le 0.1$, the model agrees well with the data. For $\beta \sim 0.1$, $\rho \sim 0.1$ to satisfy $\gamma' > 1$ and the maximum ε factor becomes $\sim$20. For $\beta \sim 0.001$, $\rho \sim 0$, $\gamma \sim C \sim 100$, and the PLE effect is very weak; thus, the ε factor goes to <5 because the term with β in the denominator of Eq. (1), which implies the cyclic A^0 accumulation effect, is negligible. When ρ is not negligible but small, therefore, the PLE effect is prominent due to the prominent contribution of the cyclic A^0 accumulation effect.

Our method for selectively amplifying the primary exciton with cavity-free tunability can open a shortcut to realize high-performance TMD optoelectronics. Moreover, our finding that exciton-coupled plasmons excite mostly the primary exciton among exciton complexes provides a deeper understanding of the complicated emission behavior of excitons in different TMDs.

This work was supported by IBS-R011-D1.

*Corresponding author.
hs.lee@skku.edu
†Corresponding author.
leeyoung@skku.edu
‡Corresponding author.
j.kim@skku.edu

[1] L. Britnell, R. M. Ribeiro, A. Eckmann, R. Jalil, B. D. Belle, A. Mishchenko, Y. J. Kim, R. V. Gorbachev, T. Georgiou, S. V. Morozov, A. N. Grigorenko, A. K. Geim, C. Casiraghi, A. H. C. Neto, and K. S. Novoselov, Science **340**, 1311 (2013).

[2] J. S. Ross, P. Klement, A. M. Jones, N. J. Ghimire, J. Q. Yan, D. G. Mandrus, T. Taniguchi, K. Watanabe, K. Kitamura, W. Yao, D. H. Cobden, and X. D. Xu, Nat. Nanotechnol. **9**, 268 (2014).

[3] S. Najmaei, Z. Liu, W. Zhou, X. L. Zou, G. Shi, S. D. Lei, B. I. Yakobson, J. C. Idrobo, P. M. Ajayan, and J. Lou, Nat. Mater. **12**, 754 (2013).

[4] S. Z. Butler, S. M. Hollen, L. Y. Cao, Y. Cui, J. A. Gupta, H. R. Gutierrez, T. F. Heinz, S. S. Hong, J. X. Huang, A. F.

Ismach, E. Johnston-Halperin, M. Kuno, V. V. Plashnitsa, R. D. Robinson, R. S. Ruoff, S. Salahuddin, J. Shan, L. Shi, M. G. Spencer, M. Terrones, W. Windl, and J. E. Goldberger, ACS Nano **7**, 2898 (2013).
[5] C. H. Cho, C. O. Aspetti, M. E. Turk, J. M. Kikkawa, S. W. Nam, and R. Agarwal, Nat. Mater. **10**, 669 (2011).
[6] G. Eda and S. A. Maier, ACS Nano **7**, 5660 (2013).
[7] J. D. Lin, H. Li, H. Zhang, and W. Chen, Appl. Phys. Lett. **102**, 203109 (2013).
[8] A. Sobhani, A. Lauchner, S. Najmaei, C. Ayala-Orozco, F. F. Wen, J. Lou, and N. J. Halas, Appl. Phys. Lett. **104**, 031112 (2014).
[9] P. Berini and I. De Leon, Nat. Photonics **6**, 16 (2012).
[10] M. S. Tame, K. R. McEnery, S. K. Ozdemir, J. Lee, S. A. Maier, and M. S. Kim, Nat. Phys. **9**, 329 (2013).
[11] C. J. Zhang, H. N. Wang, W. M. Chan, C. Manolatou, and F. Rana, Phys. Rev. B **89**, 205436 (2014).
[12] J. S. Ross, S. F. Wu, H. Y. Yu, N. J. Ghimire, A. M. Jones, G. Aivazian, J. Q. Yan, D. G. Mandrus, D. Xiao, W. Yao, and X. D. Xu, Nat. Commun. **4**, 1474 (2013).
[13] K. F. Mak, C. Lee, J. Hone, J. Shan, and T. F. Heinz, Phys. Rev. Lett. **105**, 136805 (2010).
[14] K. F. Mak, K. L. He, C. Lee, G. H. Lee, J. Hone, T. F. Heinz, and J. Shan, Nat. Mater. **12**, 207 (2013).
[15] S. Mouri, Y. Miyauchi, and K. Matsuda, Nano Lett. **13**, 5944 (2013).
[16] E. J. Sie, Y.-H. Lee, A. J. Frenzel, J. Kong, and N. Gedik, arXiv:1312.2918v1.
[17] K. P. Dhakal, D. L. Duong, J. Lee, H. Nam, M. Kim, M. Kan, Y. H. Lee, and J. Kim, Nanoscale **6**, 13028 (2014).
[18] See Supplemental Material at http://link.aps.org/supplemental/10.1103/PhysRevLett.115.226801, which includes Supplemental Refs. [19–29], for additional details on sample preparation, optical characteraization, supporting experiments, numerical simulations, analytical model, and band-filling effects.
[19] G. H. Han, N. J. Kybert, C. H. Naylor, B. S. Lee, J. Ping, J. H. Park, J. Kang, S. Y. Lee, Y. H. Lee, R. Agarwal, and A. T. C. Johnson, Nat. Commun. **6**, 6128 (2015).
[20] C. Gong, L. Colombo, R. M. Wallace, and K. Cho, Nano Lett. **14**, 1714 (2014).
[21] K. M. Goodfellow, R. Beams, C. Chakraborty, L. Novotny, and A. N. Vamivakas, Optica **1**, 149 (2014).
[22] C. Mai, A. Barrette, Y. Yu, Y. G. Semenov, K. W. Kim, L. Cao, and K. Gundogdu, Nano Lett. **14**, 202 (2014).
[23] Y. P. Wang, Y. G. Ma, X. Guo, and L. M. Tong, Opt. Express **20**, 19006 (2012).
[24] M. Allione, V. V. Temnov, Y. Fedutik, U. Woggon, and M. V. Artemyev, Nano Lett. **8**, 31 (2008).
[25] V. V. Temnov, U. Woggon, J. Dintinger, E. Devaux, and T. W. Ebbesen, Opt. Lett. **32**, 1235 (2007).
[26] X. Guo, M. Qiu, J. Bao, B. J. Wiley, Q. Yang, X. Zhang, Y. Ma, H. Yu, and L. Tong, Nano Lett. **9**, 4515 (2009).
[27] S. L. Li, H. Miyazaki, H. Song, H. Kuramochi, S. Nakaharai, and K. Tsukagoshi, ACS Nano **6**, 7381 (2012).
[28] P. Muhlschlegel, H. J. Eisler, O. J. F. Martin, B. Hecht, and D. W. Pohl, Science **308**, 1607 (2005).
[29] Y. M. Kang, S. Najmaei, Z. Liu, Y. J. Bao, Y. M. Wang, X. Zhu, N. J. Halas, P. Nordlander, P. M. Ajayan, J. Lou, and Z. Y. Fang, Adv. Mater. **26**, 6467 (2014).
[30] A. Giugni, B. Torre, A. Toma, M. Francardi, M. Malerba, A. Alabastri, R. P. Zaccaria, M. I. Stockman, and E. Di Fabrizio, Nat. Nanotechnol. **8**, 845 (2013).
[31] Y. Fedutik, V. V. Temnov, O. Schops, U. Woggon, and M. V. Artemyev, Phys. Rev. Lett. **99**, 136802 (2007).
[32] A. V. Akimov, A. Mukherjee, C. L. Yu, D. E. Chang, A. S. Zibrov, P. R. Hemmer, H. Park, and M. D. Lukin, Nature (London) **450**, 402 (2007).
[33] H. S. Lee, M. S. Kim, Y. Jin, G. H. Han, Y. H. Lee, and J. Kim, Adv. Opt. Mater. **3**, 943 (2015).
[34] J. Shang, X. Shen, C. Cong, N. Peimyoo, B. Cao, M. Eginligil, and T. Yu, ACS Nano **9**, 647 (2015).
[35] J. S. Manser and R. V. Kamat, Nat. Photonics **8**, 737 (2014).
[36] S. Hunsche, K. Leo, H. Kurz, and K. Kohler, Phys. Rev. B **49**, 16565 (1994).
[37] H. Wang, C. Zhang, and F. Rana, Nano Lett. **15**, 339 (2015).
[38] A. K. M. Newaz, D. Prasai, J. I. Ziegler, D. Caudel, S. Robinson, R. F. Haglund, and K. I. Bolotin, Solid State Commun. **155**, 49 (2013).
[39] S. F. Wu, S. Buckley, J. R. Schaibley, L. F. Feng, J. Q. Yan, D. G. Mandrus, F. Hatami, W. Yao, J. Vuckovic, A. Majumdar, and X. D. Xu, Nature (London) **520**, 69 (2015).
[40] H. Ditlbacher, A. Hohenau, D. Wagner, U. Kreibig, M. Rogers, F. Hofer, F. R. Aussenegg, and J. R. Krenn, Phys. Rev. Lett. **95**, 257403 (2005).
[41] Y. C. Jun, R. D. Kekatpure, J. S. White, and M. L. Brongersma, Phys. Rev. B **78**, 153111 (2008).
[42] D. B. Li and C. Z. Ning, Phys. Rev. B **80**, 153304 (2009).
[43] A. W. Sanders, D. A. Routenberg, B. J. Wiley, Y. N. Xia, E. R. Dufresne, and M. A. Reed, Nano Lett. **6**, 1822 (2006).